

Stacking Fault Energy Prediction for Austenitic Steels by Thermodynamic Modeling and Machine Learning

Xin Wang, Wei Xiong *

*Physical Metallurgy and Materials Design Laboratory,
Department of Mechanical Engineering and Materials Science,
University of Pittsburgh, Pittsburgh, PA 15261, USA*

* Corresponding author: wxiong@yahoo.com, weixiong@pitt.edu

Abstract

Stacking fault energy (SFE) is vital in controlling the deformation mechanism and mechanical properties of austenitic steels, while there are no accurate and straightforward computational tools for modeling it. To address this issue, we evaluate the CALPHAD-based thermodynamic models (CALPHAD: calculations of phase diagrams), analyze the alloying effect on SFE using data analytics, and present how machine learning (ML) accurately predicts the SFE of austenitic steels. The results show that ML is more precise and flexible compared to thermodynamic and empirical models. This work demonstrates the capability of ML to predict material properties when physical models and experiments are unfeasible.

Keywords: Machine learning, Stacking fault energy, Austenitic steels, CALPHAD

Designing alloys with high strength and excellent ductility is one of the ultimatums to be achieved in materials research. A plausible solution to achieve this goal is introducing the secondary deformation mechanisms, including twinning-induced plasticity (TWIP) and transformation-induced plasticity (TRIP), which continuously improve the strength and ductility during deformation [1,2]. Stacking fault energy (SFE) is the energy related to dissociating a perfect dislocation into two partial dislocations along with the formation of a stacking fault. SFE is an accurate indicator to predict which type of secondary deformation mechanism operates. Generally, TRIP activates when SFE is lower than 20 mJ/m² [3] and TWIP is achievable if the SFE lies between 20 – 40 mJ/m² [4]. Therefore, various efforts have been made to determine the SFE of different alloys. Experimental methods, including transmission electron microscopy [5–7] and X-Ray/Neutron diffraction [8,9], are tedious and difficult which delay the process of exploring new materials. Computational methods such as empirical equations, *ab initio* calculations and thermodynamic models serve as an alternative solution. Although, various empirical equations have been proposed [10–16], they predict conflicting effects for different alloying elements on SFE. This is because they are localized for a confined composition space and cannot be extrapolated for other steels. A thermodynamic model was proposed by Olson *et al.* [17], and has been adapted in many works [18–21]. Within this approach, an intrinsic stacking fault is defined as an hcp phase with two boundaries shared with the fcc matrix. However, the thermodynamic model involves many parameters and varies in different reports. Also, and none of the thermodynamic models have been verified for alloys with a broader composition range [18,21–23]. Lastly, *ab initio* methods [24,25] are difficult due to the chemical and magnetic disorder in complex alloys, and certain works underestimate the SFE and report negative values [26,27]. Thus, they are sometimes limited in predicting trends rather than the accurate value of SFE.

A promising way to leverage the wealth of data and circumvent the difficulty of SFE prediction is applying data-driven methods. Machine learning (ML) is useful in extracting knowledge from multi-dimensional data and modeling the relationships between the targeted property and its related features [28]. In recent years, there are few studies that applied ML for SFE prediction [29,30]. Das [29] predicted SFE using an artificial neural network (ANN) with 100 compositions as an input. However, that work did not incorporate temperature into the model and ANN requires an extensive database for generating a reliable model, which may limit the accuracy of this work. Chaudhary *et al.* [30] built a classifier that categorizes compositions

into high, medium and low SFE. However, the prediction of the actual SFE value is desired since it is related to model the critical stress for twinning and the mechanical properties [31,32]. Thus, a systematic study for understanding the relationship between composition and SFE, and building an accurate SFE predictor are imperative. In this paper, the following has been accomplished: 1) established a database containing the composition and SFE of various steels, 2) assessed the CALPHAD-based thermodynamic model (CALPHAD: calculations of phase diagrams), 3) discussed the influence of alloying elements on SFE, and 4) predicted SFE using ML. The performance of the ML model developed in this work is superior to the thermodynamic and empirical models. This model will serve as a valuable tool for designing TWIP/TRIP steels, and it calls for a more comprehensive database to improve the model performance and broaden the application for other alloys.

Figure 1 depicts the framework used in this work. We firstly performed an extensive literature survey and constructed a database containing 349 entries with temperature, composition, and experimentally measured SFE from 51 literatures [5–9,11,14,15,17,21,33–73]. Further, we randomly split them into train and test datasets. Our dataset covered a broad range of compositions and its descriptive statistics are listed in Table 1. Secondly, all entries in this database were screened by the thermodynamic model to calculate the SFE using Eq. 1 [17,21]:

$$\gamma = 2\rho\Delta G^{fcc\rightarrow hcp} + 2\sigma^{fcc/hcp}, \quad \rho = \frac{4}{\sqrt{3}a_{fcc}^2} \frac{1}{N_A} \quad (1)$$

where γ is the SFE (mJ/m^2), $\Delta G^{fcc\rightarrow hcp}$ is the Gibbs energies difference between the fcc and hcp phases [74]. Thermo-Calc [75] software along with TCFE9 and TCHEA3 databases were used to calculate the Gibbs energy. These commercial databases may be the most comprehensive and reliable databases for multi-component alloys compared with databases reported in literatures which were usually designed for specific steels. ρ is the molar surface density (mol/m^2) of $\{111\}$ plane, N_A is the Avogadro's number, $a_{fcc} = 0.36 \text{ nm}$ is the lattice parameter of fcc, $\sigma^{fcc/hcp} = 8 \text{ mJ}/\text{m}^2$ is interfacial energy [74]. Furthermore, we performed Spearman's correlation analysis using Python [76] and SciPy [77] to find the influence of the elements on SFE. Three different sets of features named as Standard, WithTCFE9, and WithTCHEA3 were built to find out whether the thermodynamic model can help ML model to make a better prediction. Because, an appropriate selection of features, which distinguish the material and describe the property of interest, can lead to better performance of the ML model. Further, we evaluated the performance of 19 algorithms available in Scikit-learn [78] with different hyper-parameters for the three different feature sets using the 10-fold cross-validation (CV) [79] to discover the model with highest accuracy and generalizability. In this process, the 75% train data is randomly split into ten subsets and the model is fitted with nine subgroups and tested with the remaining subgroup. After training and testing for 10 times, the average value of metrics such as the root mean square error (RMSE) and mean absolute error (MAE) were calculated using Eq. 2 and 3, respectively:

$$RMSE = \sqrt{\frac{\sum_{i=1}^n (SFE_i^E - SFE_i^P)^2}{n}} \quad (2)$$

$$MAE = \sqrt{\frac{\sum_{i=1}^n |SFE_i^E - SFE_i^P|}{n}} \quad (3)$$

where n is the number of datapoints in the evaluation, SFE_i^E and SFE_i^P are the experimental and predicted SFE of the datapoint i , respectively. Finally, the model with lowest RMSE was selected and compared with the empirical and thermodynamic models.

Evaluation of the thermodynamic model is presented in Fig. 2. Although, some points lie in the black dash line in Figs. 2(a) and 2(b), which indicates a good agreement between the thermodynamic model calculated SFE (SFE_{calc}) and SFE inferred from experiments (SFE_{exp}), but many other datapoints show a large deviation. Moreover, SFE_{exp} varies from 3 to 80 mJ/m^2 , while SFE_{calc} with TCFE9 varies between -100 to

150 mJ/m². Further, in the case of TCHEA3, the predicted values were as high as 800 mJ/m². The large discrepancy between SFE_{calc} and SFE_{exp} may originate due to the following reasons. First, the interfacial energy used in this work and other reports is considered as a constant, while it is a composition-dependent variable. Also, the difference in interfacial energy among previous studies differs by more than 20 mJ/m², which could introduce a large uncertainty [2,20,22,80–82]. Secondly, most SFE measurements are performed at room temperature while the low-temperature thermodynamic databases for multicomponent systems lack precision and the current works mainly focus on the pure element and binary reassessment [83,84]. Additionally, the magnetic contribution to SFE is significant at low temperatures and there is need for establishing a robust and sophisticated magnetic model to improve the accuracy of the thermodynamic model [85,86]. Though, the thermodynamic model is not applicable for all steels tested in this work, it is useful for certain alloy systems. According to Fig. 2(c), the two databases generate a good prediction for multiple alloy systems. For TCFE9, the error in Fe-Mn-Si-Al, Fe-Mn-Si, and Fe-Mn-Al systems are relatively small. For TCHEA3, the error in Fe-Cr-Ni, Fe-Cr-Mo-Ni and Fe-Mn systems is acceptable. The Spearman's correlation coefficient (r) for SFE_{calc} and SFE_{exp} are shown in Fig. 2(d). The r lies between -1 to 1, and represents the linear relationship between two variables. A positive value corresponds to a positive linear relation, a negative value indicates negative linear relationship, and 0 denotes that the two variables are not linearly related. For Fe-Mn-Si-Al, Fe-Mn-Al and Fe-Cr-Mn-Ni systems, the r values between SFE_{exp} and SFE_{calc} using TCFE9 are higher than 0.5, which indicates TCFE9 can predict the trend of SFE change with different elements in steels containing Mn. While, for the Fe-Cr-Ni system, TCHEA3 performs better with r value around 0.75 indicating that it is suitable for steels with high Cr and Ni. In summary, the performance of thermodynamic model heavily depends on the quality of thermodynamic databases, and should be carefully chosen depending on the alloy composition.

Understanding the influence of alloying elements on SFE is crucial for alloy design and has attracted various studies [5,27,87]. However, due to the limited time and resources, previous work only focused on limited alloys to draw a conclusion. Vitos *et al.* [24] pointed that the alloying effect on SFE is a function of both alloying element content and the host composition. Thus, the general influence of elements on SFE remains unclear. Here, we calculated the Spearman's r for interpreting the relationship between each element and the SFE without considering the host composition. According to Fig. 3, Ni has the most pronounced effect in increasing the SFE regardless of the host composition which agrees with the analysis by Das [29]. It was reported that from a total of 19 literatures, 18 reports indicated an increasing effect while only one report gave the opposite view. C and Mn do not show a strong effect of increasing/decreasing the SFE based on our study, since the r value is close to 0 and the p-value is larger than 0.05 which confirms that C and Mn does not have a statistically significant linear relationship with SFE. However, as observed in Fig. 3(b), C and Mn are important for the SFE predictor generated through gradient boosting (GB) algorithm [88]. This is because the effect of these elements on SFE is more complex than Ni and varies with different content and host alloy, which has also been verified by the literature summarization [29]. However, for some of the elements such as Si [7,44] which is generally considered to decrease the SFE, we get a contradictory conclusion, which may be attribute to the collective effect from the data pertaining to different alloy systems. When building the ML model, a 10-fold CV is used to ensure that the model can accurately predict the SFE for data untouched by the ML model. Table 2 summarizes the mean RMSE and MAE of the 10-fold CV for each model with optimized hyper-parameters. We found that the ensembled tree algorithms, including random forest [89], GB and XGBoost [90] algorithms, generate a more accurate model than other algorithms tested in this work. The GB model achieves a MAE less than 2.5 mJ/m² for all of the input sets. The RMSE which is sensitive to large prediction errors, is nearly 8 mJ/m². This implies that some large deviation happens during the prediction. However, the overall performance is still reasonable. In our study, the ensembled methods always performs better than the multilayer perception (MLP, an ANN model)[91] based on different metrics, indicating our hypothesis that there are better algorithms for predicting SFE than ANN as stated in the introduction. We also found that the overall performance is similar among the three input sets. Although the performance of adding TCFE9 calculated SFE is slightly better than the standard

inputs, the improvement is minor. As a result, addition of thermodynamic calculations does not greatly benefit the ML model.

Finally, the GB algorithm with optimized hyper-parameters was re-trained with 75% data and tested with untouched 25% data. According to Fig. 4(a), almost all the data in the train dataset align with the black dash line, which represent the prediction is the same as experiments. This implies that the ML model successfully correlates the composition and temperature to SFE for the train dataset. This model also performs good on the untouched test dataset, except for one outlier. Based on the inset plot, it is clear that more than 70% of the prediction error is less than 10 mJ/m², which is close to the experimental error [16,47]. The error in SFE inferred from experiments may come from the equipment used for characterization, the inherent variation of SFE within a sample [35,92], and inaccurate elastic constants used when deducing SFE from experimental observation [6,21]. The performance of ML, thermodynamic and empirical models on the test dataset are compared, and the results are shown in Fig. 4(b). Equation 4 proposed by Bellefon [16] is so far the most accurate empirical model available [10–15]. It is clear that the MAE and RMSE of ML models are smallest amongst the empirical and thermodynamic models confirming that ML is the most capable model for SFE prediction.

$$\gamma(\text{mJ}/\text{m}^2) = 2.2 + 1.9\text{Ni} - 2.9\text{Si} + 0.7\text{Mo} + 0.5\text{Mn} + 40\text{C} - 0.016\text{Cr} - 3.6\text{N} \quad (4)$$

The advantage of a ML model is not only higher accuracy, but also its ability to continuously evolve. Once the SFE measurements are reported, the data can be incorporated in the current dataset to gain an improved prediction [93,94]. Also, if new features such as the heat treatment process, the grain size, and the accurate prediction of interfacial energy and magnetic contribution are incorporated, the performance can be also potentially improved.

In summary, we evaluated the thermodynamic model for SFE prediction, revealed the influence of alloying elements on SFE with statistical analysis, and built an accurate SFE model using ML. We found that there is a need to reassess the low-temperature multi-component thermodynamic databases, and incorporate better magnetic and interfacial energy models to the thermodynamic model. According to literature and Spearman's correlation analysis, it was found that Ni has a monotonous relationship on SFE for most steels. While elements like C and Mn show complex effects on SFE, which are usually related to the alloying element content and the host composition. The GB algorithm performs best among the thermodynamic and empirical models, which proves the advantages of applying ensembled methods for SFE prediction. Based on these results, we envisage that the data-driven method presented in this work will accelerate alloy design through optimization of SFE to yield preferred deformation mechanisms and excellent mechanical properties.

Acknowledgments

W.X. acknowledges funding from the National Science Foundation under award DMR - 1808082, and from the University of Pittsburgh, through the Central Research Development Fund (CRDF). The authors are grateful for helpful discussions with Dr. Soumya Sridar, Mr. Rafael Tomás Rodríguez De Vecchis, and Mr. Noah Sargent at the University of Pittsburgh.

References

- [1] O. Grässel, L. Krüger, G. Frommeyer, L.W. Meyer, *Int. J. Plast.* 16 (2000) 1391–1409.
- [2] D.R. Steinmetz, T. Jäpel, B. Wietbrock, P. Eisenlohr, I. Gutierrez-Urrutia, A. Saeed-Akbari, T. Hickel, F. Roters, D. Raabe, *Acta Mater.* 61 (2013) 494–510.
- [3] K. Sato, M. Ichinose, Y. Hirotsu, Y. Inoue, *ISIJ Int.* 29 (1989) 868–877.
- [4] J. Su, D. Raabe, Z. Li, *Acta Mater.* 163 (2019) 40–54.
- [5] J. Lu, L. Hultman, E. Holmström, K.H. Antonsson, M. Grehk, W. Li, L. Vitos, A. Golpayegani,

- Acta Mater. 111 (2016) 39–46.
- [6] D.T. Pierce, J. Bentley, J.A. Jiménez, J.E. Wittig, *Scr. Mater.* 66 (2012) 753–756.
 - [7] G.R. Lehnhoff, K.O. Findley, B.C. De Cooman, *Scr. Mater.* 92 (2014) 19–22.
 - [8] J. Kim, B.C. De Cooman, *Metall. Mater. Trans. A* 42 (2011) 932–936.
 - [9] T.H. Lee, E. Shin, C.S. Oh, H.Y. Ha, S.J. Kim, *Acta Mater.* 58 (2010) 3173–3186.
 - [10] R.E. Schramm, R.P. Reed, *Metall. Trans. A* 6 (1975) 1345.
 - [11] C.G. Rhodes, A.W. Thompson, *Metall. Trans. A* 8 (1977) 1901–1906.
 - [12] P.J. Brofman, G.S. Ansell, *Metall. Mater. Trans. A* 9 (1978) 879–880.
 - [13] D. Qi-Xun, W. An-Dong, C. Xiao-Nong, L. Xin-Min, *Chinese Phys.* 11 (2002) 596.
 - [14] M. Ojima, Y. Adachi, Y. Tomota, Y. Katada, Y. Kaneko, K. Kuroda, H. Saka, *Steel Res. Int.* 80 (2009) 477–481.
 - [15] T. Yonezawa, K. Suzuki, S. Ooki, A. Hashimoto, *Metall. Mater. Trans. A* 44 (2013) 5884–5896.
 - [16] G.M. de Bellefon, J.C. van Duysen, K. Sridharan, *J. Nucl. Mater.* 492 (2017) 227–230.
 - [17] G.B. Olson, M. Cohen, *Metall. Trans. A* 7 (1976) 1897–1904.
 - [18] S. Curtze, V.-T. Kuokkala, *Acta Mater.* 58 (2010) 5129–5141.
 - [19] S.-J. Lee, Y. Sun, H. Fujii, *Acta Mater.* 148 (2018) 235–248.
 - [20] A. Saeed-Akbari, J. Imlau, U. Prahl, W. Bleck, *Metall. Mater. Trans. A Phys. Metall. Mater. Sci.* 40 (2009) 3076–3090.
 - [21] D.T. Pierce, J.A. Jiménez, J. Bentley, D. Raabe, C. Oskay, J.E. Wittig, *Acta Mater.* 68 (2014) 238–253.
 - [22] L. Mosecker, A. Saeed-Akbari, *Sci. Technol. Adv. Mater.* 14 (2013).
 - [23] D. Djurovic, B. Hallstedt, J. Von Appen, R. Dronskowski, *Calphad* 35 (2011) 479–491.
 - [24] L. Vitos, J.-O. Nilsson, B. Johansson, *Acta Mater.* 54 (2006) 3821–3826.
 - [25] S. Huang, W. Li, S. Lu, F. Tian, J. Shen, E. Holmström, L. Vitos, *Scr. Mater.* 108 (2015) 44–47.
 - [26] D. Wei, X. Li, J. Jiang, W. Heng, Y. Koizumi, W.-M. Choi, B.-J. Lee, H.S. Kim, H. Kato, A. Chiba, *Scr. Mater.* 165 (2019) 39–43.
 - [27] S. Kibey, J.B. Liu, M.J. Curtis, D.D. Johnson, H. Sehitoglu, *Acta Mater.* 54 (2006) 2991–3001.
 - [28] Y. Liu, T. Zhao, W. Ju, S. Shi, *J. Mater.* 3 (2017) 159–177.
 - [29] A. Das, *Metall. Mater. Trans. A Phys. Metall. Mater. Sci.* 47 (2016) 748–768.
 - [30] N. Chaudhary, A. Abu-Odeh, I. Karaman, R. Arróyave, *J. Mater. Sci.* 52 (2017) 11048–11076.
 - [31] S. Kibey, J.B. Liu, D.D. Johnson, H. Sehitoglu, *Acta Mater.* 55 (2007) 6843–6851.
 - [32] G.M. de Bellefon, M.N. Gussev, A.D. Stoica, J.C. van Duysen, K. Sridharan, G. Meric de Bellefon, M.N. Gussev, A.D. Stoica, J.C. van Duysen, K. Sridharan, *Scr. Mater.* 157 (2018) 162–166.
 - [33] F. Abrassart, *Metall. Trans.* 4 (1973) 2205–2216.
 - [34] C.C. Bampton, I.P. Jones, M.H. Loretto, *Acta Metall.* 26 (1978) 39–51.
 - [35] P. Behjati, A. Najafizadeh, *Metall. Mater. Trans. A* 42 (2011) 3752.
 - [36] J.T. Benzing, W.A. Poling, D.T. Pierce, J. Bentley, K.O. Findley, D. Raabe, J.E. Wittig, *Mater. Sci. Eng. A* 711 (2018) 78–92.
 - [37] L. Bracke, J. Penning, N. Akdut, *Metall. Mater. Trans. A* 38 (2007) 520–528.
 - [38] D. Dulieu, *Spec. Rep.* 86 140 (1964).
 - [39] R. Fawley, M.A. Quader, R.A. Dodd, *Trans Met Soc AIME* 242 (1968) 771–776.
 - [40] V. Gavriljuk, Y. Petrov, B. Shanina, *Scr. Mater.* 55 (2006) 537–540.

- [41] V.G. Gavriljuk, A.L. Sozinov, J. Foct, J.N. Petrov, Y.A. Polushkin, *Acta Mater.* 46 (1998) 1157–1163.
- [42] H. Idrissi, K. Renard, L. Ryelandt, D. Schryvers, P.J. Jacques, *Acta Mater.* 58 (2010) 2464–2476.
- [43] L.G. Martinez, K. Imakuma, A.F. Padilha, *Steel Res.* 63 (1992) 221–223.
- [44] K. Jeong, J.E. Jin, Y.S. Jung, S. Kang, Y.K. Lee, *Acta Mater.* 61 (2013) 3399–3410.
- [45] Z. Jiao, G.S. Was, *J. Nucl. Mater.* 407 (2010) 34–43.
- [46] M. Kang, W. Woo, Y.-K. Lee, B.-S. Seong, *Mater. Lett.* 76 (2012) 93–95.
- [47] J. Kim, S.-J. Lee, B.C. De Cooman, *Scr. Mater.* 65 (2011) 363–366.
- [48] R.M. Latanision, A.W. Ruff, *Metall. Trans.* 2 (1971) 505–509.
- [49] F. Lecroisey, B. Thomas, *Phys. Status Solidi* 2 (1970) K217–K220.
- [50] F. Lecroisey, A. Pineau, *Metall. Mater. Trans. B* 3 (1972) 391–400.
- [51] T.-H. Lee, H.-Y. Ha, B. Hwang, S.-J. Kim, E. Shin, *Metall. Mater. Trans. A* 43 (2012) 4455–4459.
- [52] S.J. Lee, Y.S. Jung, S. Il Baik, Y.W. Kim, M. Kang, W. Woo, Y.K. Lee, *Scr. Mater.* 92 (2014) 23–26.
- [53] J.C. Li, W. Zheng, Q. Jiang, *Mater. Lett.* 38 (1999) 275–277.
- [54] X. Li, A. Almazouzi, *J. Nucl. Mater.* 385 (2009) 329–333.
- [55] L. Mosecker, D.T. Pierce, A. Schwedt, M. Beighmohamadi, J. Mayer, W. Bleck, J.E. Wittig, *Mater. Sci. Eng. A* 642 (2015) 71–83.
- [56] L. Mujica, S. Weber, W. Theisen, *Mater. Sci. Forum* 706–709 (2012) 2193–2198.
- [57] Y.N. Petrov, *Phys. Met.* 6 (1985) 735–741.
- [58] Y.N. Petrov, *Scr. Metall. Mater. States* 29 (1993).
- [59] Y.N. Petrov, *Zeitschrift Für Met.* 94 (2003) 1012–1016.
- [60] Y. Petrov, *Int. J. Mater. Res.* 103 (2012) 551–553.
- [61] D. Rafaja, C. Krbetschek, C. Ullrich, S. Martin, *J. Appl. Crystallogr.* 47 (2014) 936–947.
- [62] W. Reick, M. Pohl, A.F. Padilha, *ISIJ Int.* 38 (1998) 567–571.
- [63] L. Rémy, A. Pineau, B. Thomas, *Mater. Sci. Eng.* 36 (1978) 47–63.
- [64] G.S. Shin, J.Y. Yun, M.C. Park, S.J. Kim, *Tribol. Lett.* 57 (2015) 25.
- [65] J.M. Silcock, *Corrosion* 38 (1982) 144–156.
- [66] R.E. Stoltz, J.B. Vander Sande, *Metall. Trans. A* 11 (1980) 1033–1037.
- [67] J.R. Strife, M.J. Carr, G.S. Ansell, *Metall. Trans. A* 8 (1977) 1471–1484.
- [68] P.R. Swann, *Corrosion* 19 (1963) 102t–114t.
- [69] R. Taillard and J. Foct, in: A. Hendry (Eds.), *High Nitrogen Steels*, HNS 88, Inst. Met. London, 1989, p. 387.
- [70] J. Talonen, H. Hänninen, *Acta Mater.* 55 (2007) 6108–6118.
- [71] B. THOMAS, G. HENRY, J. PLATEAU, J. HOCHMANN, *COMPT REND ACAD SCI* 264 (1967) 31–34.
- [72] X. Tian, Y. Zhang, *Mater. Sci. Eng. A* 516 (2009) 73–77.
- [73] S.W. Yang, J.E. Spruiell, *J. Mater. Sci.* 17 (1982) 677–690.
- [74] S. Curtze, V.-T.T. Kuokkala, A. Oikari, J. Talonen, H. Hänninen, *Acta Mater.* 59 (2011) 1068–1076.
- [75] J.-O. Andersson, T. Helander, L. Höglund, P. Shi, B. Sundman, *Calphad* 26 (2002) 273–312.
- [76] K.J. Millman, M. Aivazis, *Comput. Sci. Eng.* 13 (2011) 9–12.
- [77] P. Virtanen, R. Gommers, T.E. Oliphant, M. Haberland, T. Reddy, D. Cournapeau, E. Burovski, P.

- Peterson, W. Weckesser, J. Bright, ArXiv Prepr. ArXiv1907.10121 (2019).
- [78] F. Pedregosa, G. Varoquaux, A. Gramfort, V. Michel, B. Thirion, O. Grisel, M. Blondel, P. Prettenhofer, R. Weiss, V. Dubourg, J. Mach. Learn. Res. 12 (2011) 2825–2830.
- [79] R. Kohavi, in: Ijcai, Montreal, Canada, 1995, pp. 1137–1145.
- [80] S. Allain, J.-P. Chateau, O. Bouaziz, S. Migot, N. Guelton, Mater. Sci. Eng. A 387 (2004) 158–162.
- [81] S.M. Cotes, A.F. Guillermet, M. Sade, Metall. Mater. Trans. A 35 (2004) 83–91.
- [82] P.U. Volosevich, V.N. Gridnev, Y.U.N. Petrov, Phys. Met. Met. 42 (1976) 126–130.
- [83] Q. Chen, B. Sundman, J. Phase Equilibria 22 (2001) 631–644.
- [84] W. Xiong, P. Hedström, M. Selleby, J. Odqvist, M. Thuvander, Q. Chen, Calphad 35 (2011) 355–366.
- [85] W. Xiong, H. Zhang, L. Vitos, M. Selleby, Acta Mater. 59 (2011) 521–530.
- [86] W. Xiong, Q. Chen, P.A. Korzhavyi, M. Selleby, Calphad 39 (2012) 11–20.
- [87] K.R. Limmer, J.E. Medvedeva, D.C. Van Aken, N.I. Medvedeva, Comput. Mater. Sci. 99 (2015) 253–255.
- [88] J.H. Friedman, Ann. Stat. (2001) 1189–1232.
- [89] L. Breiman, Mach. Learn. 45 (2001) 5–32.
- [90] T. Chen, C. Guestrin, in: Proc. 22nd Acm Sigkdd Int. Conf. Knowl. Discov. Data Min., 2016, pp. 785–794.
- [91] M.W. Gardner, S.R. Dorling, Atmos. Environ. 32 (1998) 2627–2636.
- [92] N.L. Okamoto, S. Fujimoto, Y. Kambara, M. Kawamura, Z.M.T. Chen, H. Matsunoshita, K. Tanaka, H. Inui, E.P. George, Sci. Rep. 6 (2016) 35863.
- [93] L. Ward, S.C. O’Keeffe, J. Stevick, G.R. Jelbert, M. Aykol, C. Wolverton, Acta Mater. 159 (2018) 102–111.
- [94] D. Xue, P. V Balachandran, J. Hogden, J. Theiler, D. Xue, T. Lookman, Nat. Commun. 7 (2016) 11241.

Table and Figure Captions

Table 1. Descriptive statistics of database used in this work.....	2
Table 2. Comparison of the performance of different algorithm for different input sets	3
Graphical abstract	4
Figure 1. Schematic describing the procedure of this work.....	4
Figure 2. Comparison of SFE measured by experiments (SFE_{exp}) and calculated using the thermodynamic model (SFE_{calc}) with (a) TCFE9 and (b) TCHEA3 database for different alloy systems (labeled with substitutional elements exceeding 1 wt.%), where the black dash line denotes $SFE_{calc} = SFE_{exp}$, (c) Mean value and standard deviation for the difference between SFE_{calc} and SFE_{exp} for different alloy systems, and (d) the Spearman's correlation coefficient between the SFE_{calc} and SFE_{exp} for each alloy system.....	5
Figure 3. (a) Spearman's correlation coefficient and p-value for the SFE and all features used in this work, (b) Importance of each features in gradient boosting (GB)	6
Figure 4. (a) comparison of the experimental and ML predicted SFE, the black dash line represents ideal case where prediction equals to experiment measured SFE (b) comparison for performance of machine learning, empirical model, and thermodynamic model using TCHEA3 and TCFE9 database in terms of MAE and RMSE	7

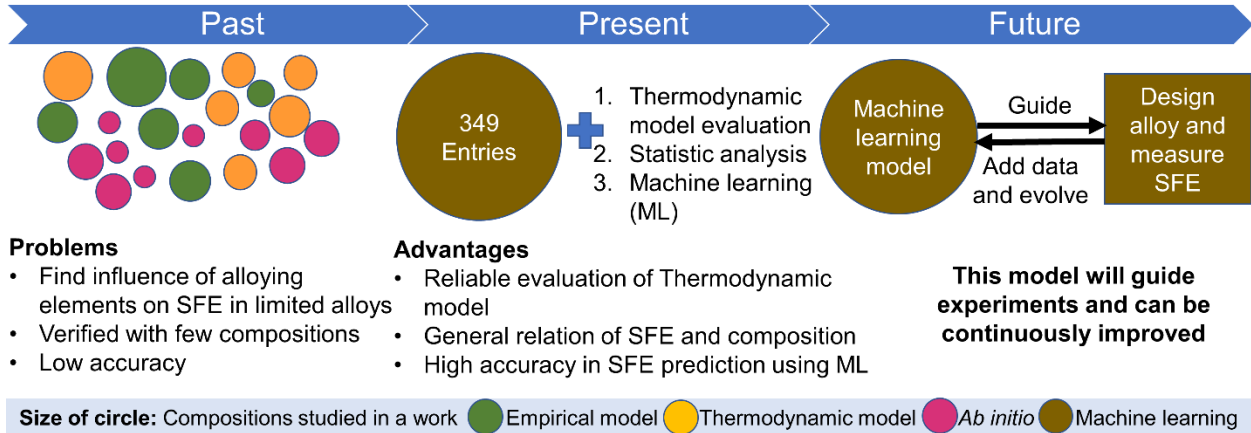
Table 1. Descriptive statistics of database used in this work

	Temperature (K)	C (wt.%)	Cr (wt.%)	Mn (wt.%)	Mo (wt.%)	N (wt.%)	Ni (wt.%)	Si (wt.%)	Al (wt.%)	P (wt.%)	S (wt.%)	Fe (wt.%)	SFE (mJ/m ²)
Mean	289.94	0.09	15.36	5.09	0.41	0.07	11.23	0.34	0.10	0.00	0.00	67.31	30.60
Standard Deviation	46.87	0.26	6.39	8.18	0.89	0.15	6.87	0.99	0.52	0.01	0.00	7.19	13.55
Min	94.30	0.00	0.00	0.00	0.00	0.00	0.00	0.00	0.00	0.00	0.00	47.04	3.26
Max	598.15	3.21	30.00	32.69	2.70	1.00	31.16	6.22	4.80	0.07	0.04	86.46	72.97

Table 2. Comparison of the performance of different algorithm for different input sets

Machine learning algorithm	Mean RMSE (mJ/m ²) of 10-fold CV			Mean MAE (mJ/m ²) of 10-fold CV		
	Standard	With TCFE9	With TCHEA3	Standard	With TCFE9	With TCHEA3
Gradient boosting	7.8	7.8	7.9	2.4	2.3	2.3
Random forest	8.0	7.9	8.1	2.4	2.4	2.4
XGBoost	8.1	8.0	8.2	2.4	2.4	2.4
Huber	9.3	9.2	9.4	2.6	2.6	2.7
Adaptive boosting	9.3	9.2	9.5	2.8	2.7	2.8
K-nearest neighbors	9.4	8.9	9.3	2.6	2.6	2.6
Elastic net	9.5	9.2	9.5	2.7	2.6	2.7
Ridge	9.5	9.3	9.5	2.7	2.7	2.7
Kernel ridge	9.5	9.3	9.5	2.7	2.7	2.7
Lasso	9.5	9.2	9.5	2.7	2.6	2.7
Automatic relevance determination	9.5	9.3	9.5	2.7	2.7	2.7
LassoLars	9.5	9.3	9.5	2.7	2.7	2.7
Extra-trees	9.5	10.5	10.0	2.7	2.7	2.7
Linear regression	9.6	9.4	9.6	2.7	2.7	2.7
Bayesian ridge	9.6	9.3	9.5	2.7	2.7	2.7
Multilayer perception	9.8	9.4	10.2	2.7	2.7	2.7
Supporting vector machine	9.8	9.3	9.7	2.7	2.6	2.6
Decision tree	10.2	10.1	10.1	2.7	2.7	2.7
Stochastic gradient descent	11.7	11.4	11.6	3.0	2.9	3.0

Approaches for Predicting Stacking Fault Energy (SFE)



Graphical abstract

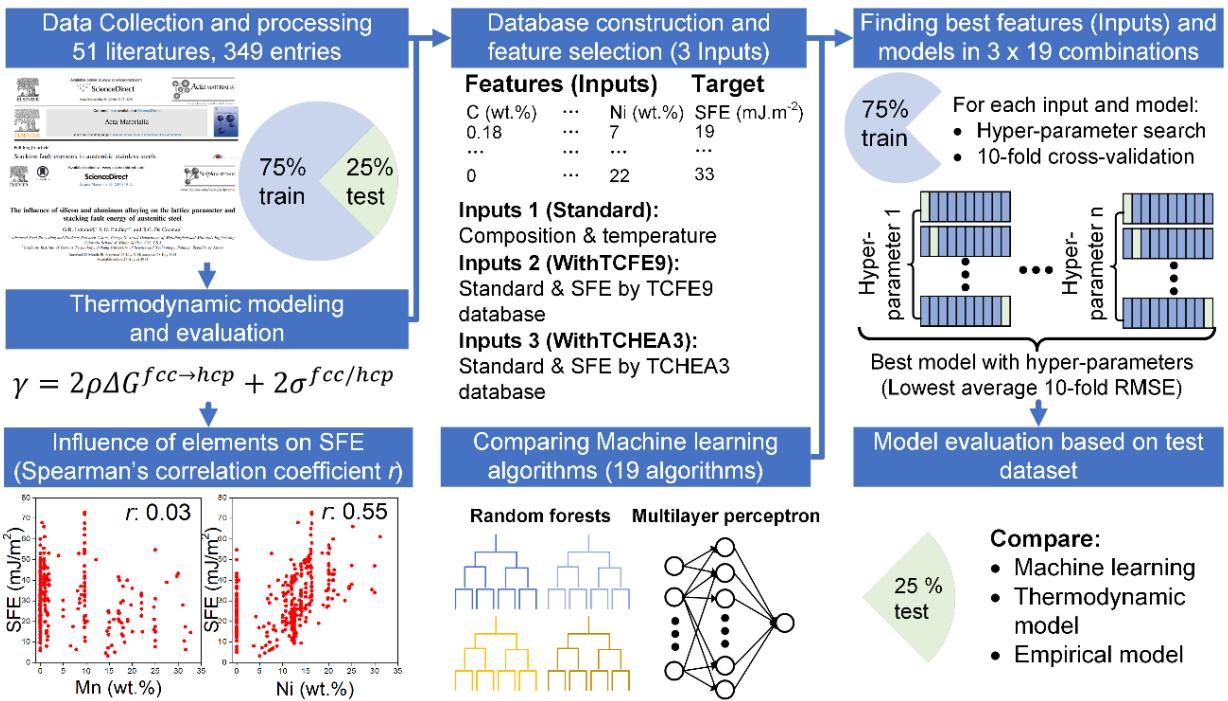


Figure 1. Schematic describing the procedure of this work

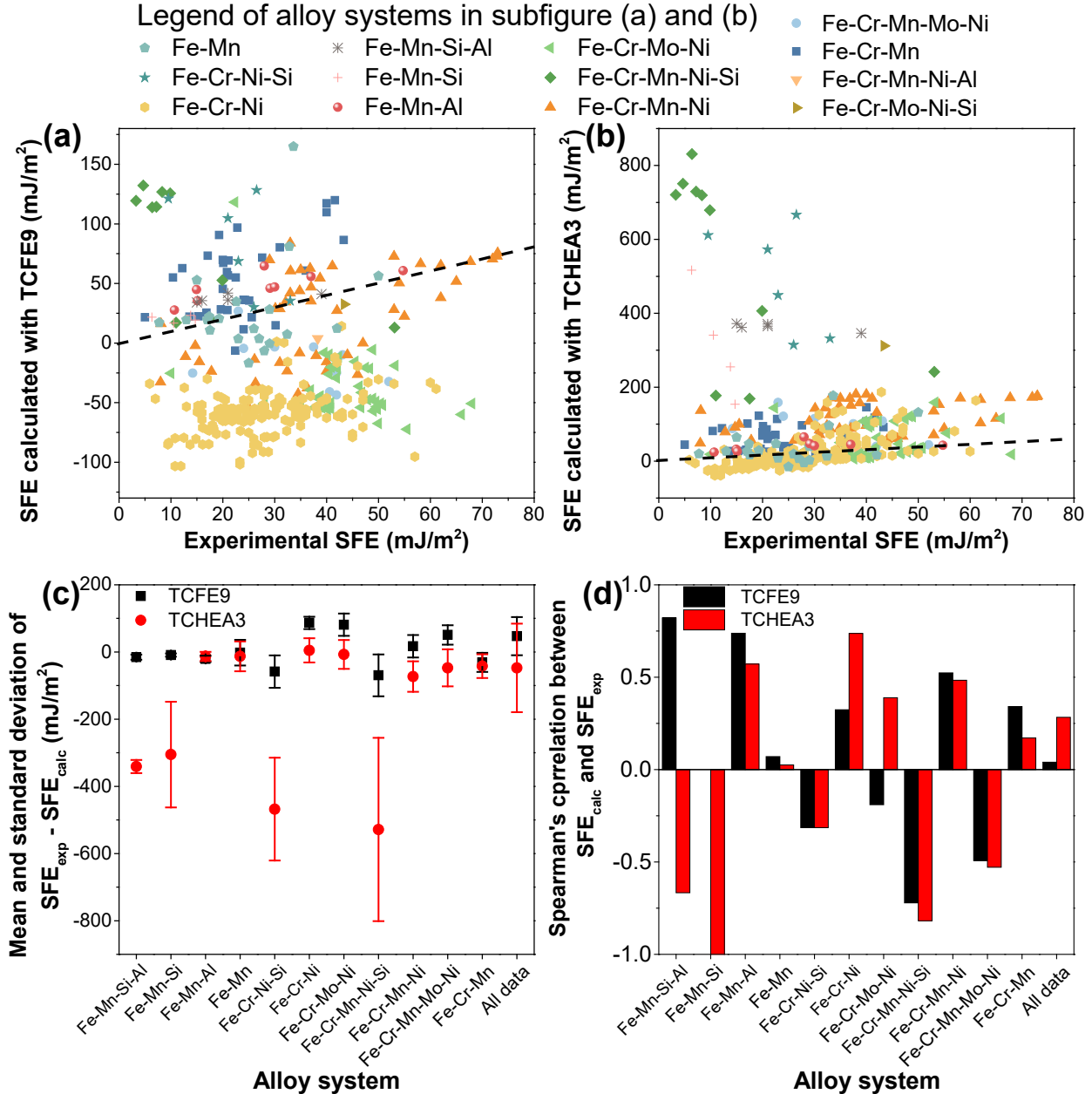


Figure 2. Comparison of SFE measured by experiments (SFE_{exp}) and calculated using the thermodynamic model (SFE_{calc}) with (a) TCFE9 and (b) TCHEA3 database for different alloy systems (labeled with substitutional elements exceeding 1 wt.%), where the black dash line denotes $\text{SFE}_{\text{calc}} = \text{SFE}_{\text{exp}}$, (c) Mean value and standard deviation for the difference between SFE_{calc} and SFE_{exp} for different alloy systems, and (d) the Spearman's correlation coefficient between the SFE_{calc} and SFE_{exp} for each alloy system

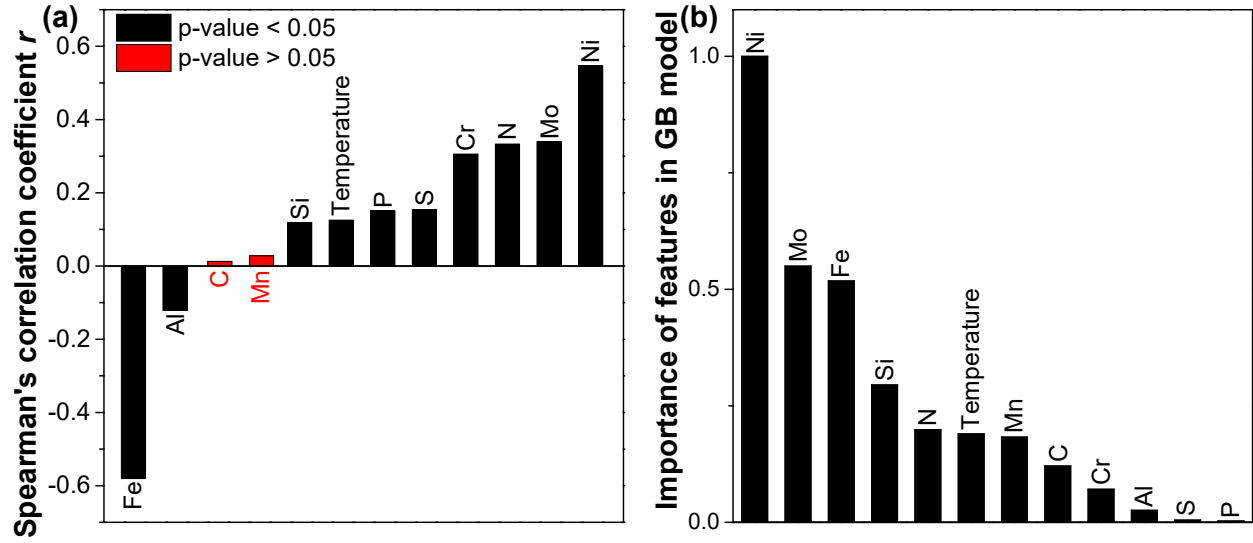


Figure 3. (a) Spearman's correlation coefficient and p-value for the SFE and all features used in this work, (b) Importance of each features in gradient boosting (GB)

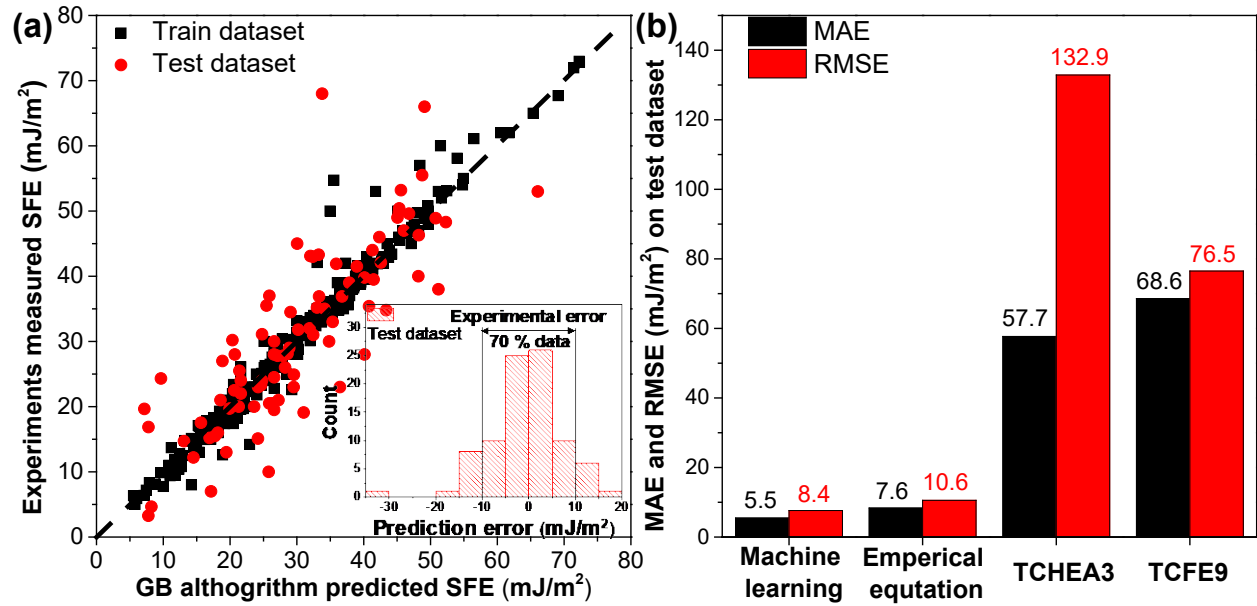


Figure 4. (a) comparison of the experimental and ML predicted SFE, the black dash line represents ideal case where prediction equals to experiment measured SFE (b) comparison for performance of machine learning, empirical model, and thermodynamic model using TCHEA3 and TCFE9 database in terms of MAE and RMSE